Thermal analysis of the ^{Po}Cat-3 PocketQube satellite

Author: Óscar Pavón Amador, opavonam11@alumnes.ub.edu
Facultat de Física, Universitat de Barcelona, Diagonal 645, 08028 Barcelona, Spain.

Advisors: Adriano Camps, Anna Maria Vilà Arbonès

Abstract: This Final Degree Project presents the thermal analysis of ^{Po}Cat-3, a 1P PocketQube satellite. The thermal behavior of the spacecraft is evaluated, validating the requirements established by its electrical components, while also providing a solid foundation for future analysis of other IEEE Open PocketQubes. A thermal model was developed based on the satellite's geometry, material properties, and orbital parameters. Simulations under transient conditions are presented for different boundary conditions. The results obtained showcase the need for an active thermal system and the potential transition from white coating to a more absorbing one, as in both cold and hot scenarios not all requirements have been found to be met due to lower than acceptable predicted temperatures.
Keywords: Heat transfer, thermal simulation, PocketQube, electronics, TCR
SDGs: ODS 4, ODS 9,ODS 13

I. INTRODUCTION

With the introduction of the CubeSat standard [1] in 1999 the number of satellites launched in the past two decades has increased exponentially.

The so called New Space has boosted the interest for smaller, cost-effective, and faster ways to produce satellites. Ultimately, this led to the creation of the PocketQube standard [2], a pico-satellite category of spacecrafts (S/Cs) of 5x5x5 cm^3 cubic shape with a maximum weight of 250 g (1P configuration). It is within this context that the IEEE GRSS PocketQube Kit was developed by the UPC NanoSat Lab, to lower the entry-point to educational institutions into the space field, and establishing an updated standard for future PocketQubes[3] (PQs).

The ^{Po}Cat-3 satellite is a 1P PQ, fully designed, manufactured, assembled and tested by the UPC NanoSat Lab, currently being worked on by the ^{Po}Cat-Lektron team, leading the IEEE GRSS OpenPocketQube Kit initiative and also supported by ESA's Fly Your Satellite 4! (FYS4!) program [4]. Its main objective is to demonstrate the feasibility to conduct scientific missions using PocketQube platforms. To do so, the mission proposes to collect data on radiofrequency interference (RFI) distribution across the globe by means of a K-band spectrum monitoring payload, to evaluate the impact on the atmospheric water vapor measurements by 5G network deployment, in the 24-25 GHz band.

Being launched together with ^{Po}Cat-2, which is equipped with an L-band spectrum monitoring payload, the mission also aims to validate that PQ platforms can create, manage and join a Federated Satellite System (FSS) [5]. Finally, it is important to acknowledge that the mission is oriented towards undergraduate and master students gaining experience, getting involved in real space missions, and has already had a significant educational impact[6].

In addition, ^{Po}Cat-1, equipped with a VGA camera payload was also developed in parallel. An image of the three PQs if shown in Figure 1.

As with any instrument of measurement, ^{Po}Cat-3 can only operate successfully under certain environmental conditions, therefore the mechanical and thermal stresses it may be subject to during its lifespan have to be studied in detail. While mechanical integrity mostly poses a mission threat during launch, the thermal requirements established by each component of the PQ are to be met, including a certain margin, for the whole mission duration. Space conditions are very difficult to be imitated on ground, and while thermal and vacuum chambers and shakers are able to reach the conditions experienced by the spacecraft, they provide insufficient data to individually validate the instrument.

In order to remedy this issue, thermal and structural analysis are performed, making use of geometrical, mathematical and physical modeling. In this work, the thermal analysis of ^{Po}Cat-3 is presented. Results are discussed in order to assess compliance with the thermal requirements established by its electrical components. The used software for simulations and modeling is ESATAN-TMS [7], a thermal modeling suite developed by ITP Aero, designed for space applications.

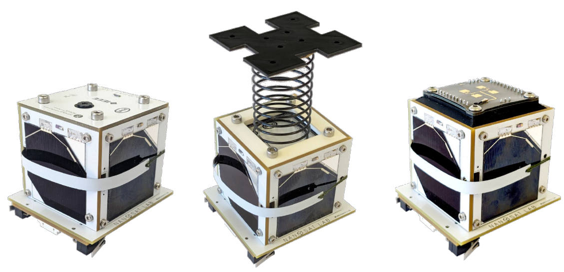

FIG. 1: ^{Po}Cat-1, equipped with a VGA camera payload, ^{Po}Cat-2 and ^{Po}Cat-3, equipped with spectrum monitoring payloads in the L-band and the K-band, respectively.

II. SYSTEM ARCHITECTURE

A. Structure and subsystems

The ^{Po}Cat-3 architecture comprises multiple functional subsystems responsible for data acquisition, communication, and overall system operation and attitude maintenance. Most electronics are mounted onto printed-circuit boards (PCBs) located at the center of the S/C. Additional PCBs mounted laterally support the solar arrays, which provide primary power, and house the magnetorquer coils for attitude control. The battery pack is positioned underneath the PCB stack and is mechanically secured and insulated by a polytetrafluoroethylene (PTFE) enclosure.

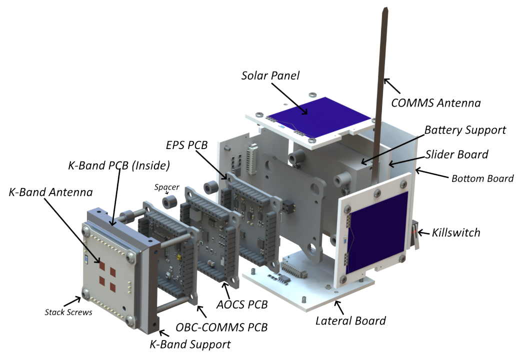

FIG. 2: Exploded, labeled, render view of ^{Po}Cat-3

Figure 2 illustrates this architecture. The subsystems, as labeled, perform the following tasks:

- **Electrical Power System (EPS)**: Power generation, distribution, and battery management.
- **Attitude & Orbit Control System (AOCS)**: Detumbling, pointing, and orbit propagation.
- **On-Board Computer (OBC)**: Data processing and handling, single microcontroller unit (MCU) in the system.
- **Communications (COMMS)**: Telemetry, tracking, and command.
- **Payload (P/L)**: Spectrum monitoring on the K-band.

An explanation of the operational modes of the satellite and their estimated power consumptions is presented in Appendix A.

B. Component temperature ranges

Each of the subsystems is built upon different integrated circuits, electrical components and mechanical supports. Therefore, in order to thermally validate the PQ, it must be ensured that all component are within their thermal thresholds.

Margins of $\pm 5\,^{\circ}$C for acceptance and $\pm 10\,^{\circ}$C for qualification, as defined in ECSS guidelines [8], are applied to the operational temperature ranges of all electrical components to account for thermal-model inaccuracies and unpredictable events. After applying these margins, and grouping them by the most limiting components of each subsystem, the design temperature ranges (DTRs) are derived, shown in Table I.

TABLE I: Design temperature ranges for subsystems and battery.

Subsystem/Component	Min (°C)	Max (°C)
EPS	–30	75
AOCS	–20	75
OBC/COMMS	–10	60
K-band	–30	75
K-band Antenna	–30	115
Lateral Boards	–30	115
Bottom Board	–30	75
Battery (Charge)	10	35
Battery (Discharge)	–10	50

III. THERMAL MODEL DESCRIPTION

On one hand, to create a feasible model, the following relevant assumptions are made:

1. All materials' thermal and optical properties are constant, under all conditions.
2. PCBs can be modeled as a parallel, and serial set of thermal resistances.
3. Electrical components can be modeled as Non-Geometrical Thermal Nodes (NGTNs) with a given thermal conductance and heat dissipation.

On the other hand, total heat transfer (Q), a sum of conductive (Q_{cond}), convective (Q_{conv}) and radiative (Q_{rad}) contributions,

$$Q = Q_{cond} + Q_{conv} + Q_{rad} \quad , \tag{1}$$

is simplified to only be significative by conduction and radiation, which will also transfer heat between internal PCBs, neglecting convective transfer due to the low density of space, yielding:

$$Q = -kA\frac{dT}{dx} + \epsilon\sigma A_s(T_s^4 - T_{env}^4) \quad , \tag{2}$$

where k and A are the conductivity and area of the heat path, A_s and T_s are the area and temperature of the surface, ϵ and σ the emissivity of the material and the Stefan-Boltzmann constant, and T_{env} is the temperature of the environment.

While many of the materials properties may be extracted from direct sources, without the need of calculations, and the corresponding mass to each primitive has been measured, the same cannot be applied for composite pieces. A comprehensive list of how such properties have been calculated can be found on Appendix B. The calculations for the PCBs yield the values of specific heat (c_p), cross-plane conductivity ($k_{c.p}$) and in-plane conductivity ($k_{i.p.}$), shown in Table II:

TABLE II: PCB Bulk Thermal Properties

PCB	c_p **(J/kg·K)**	$k_{\mathbf{c.p.}}$ **(W/m·K)**	$k_{\mathbf{i.p.}}$ **(W/m·K)**
OBC-COMMS	940	0.32	91
EPS	940	0.32	91
AOCS	940	0.32	91
Laterals	904	0.32	171
Bottom	904	0.32	171
Slider	1050	0.30	47
K-band PCB	783	0.31	110
K-band Antenna	905	0.29	89

A detailed mechanical SolidWorks CAD model [9] of ^{Po}Cat-3 has been used as reference for the elaboration of a simplified thermal model in ESATAN-TMS. All pieces have been modeled as solid rectangular prisms, as solid cylinders or as NGTNs. An overview of this modeling is presented in Figures 3 and 4, in comparison with the realistic model, while further details are provided in Appendix C.

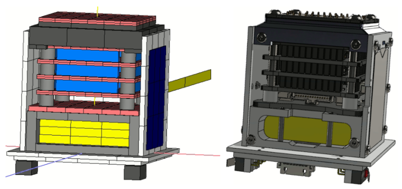

FIG. 3: ESATAN-TMS and SolidWorks models of an opened PQ

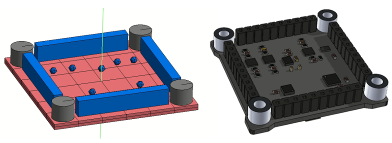

FIG. 4: ESATAN-TMS and SolidWorks models of the AOCS PCB

Due to the construction of the model, many heat paths are not represented by the intersection between primitives. To account for them, user defined conductors (UDCs or G_L) are defined, with their conductance set by material properties and shape factor, as in Eq. 3:

$$G_L = k\frac{A}{l} \quad , \tag{3}$$

where k, A and l are the conductivity, area and length of the path, respectively.

A. Thermal Contact Resistance

Thermal contact resistance (TCR) determines the heat transfer rate between two bodies in physical contact. The TCR calculation is a complex problem, and of outmost importance in the case of bolted joints. In the presented model two approaches have been taken to determine its values. On one hand, the inner stack TCRs with each of its spacers is computed by adjusting the values presented in [10] to our configuration. On the other hand, due to the lack of experimental data, an approximation of the TCR is made through the combination of Mikic's 1974 elastic deformation model [11], which yields the TCR of pressured surfaces by unit area:

$$h_c = 1.55\frac{k_s m_s}{\sigma_s}\left(\frac{P\sqrt{2}}{E' m_s}\right) \quad , \tag{4}$$

where k_s is the harmonic mean of conductivities, m_s is RMS the slope of the microcontacts, σ_s is the RMS surface roughness, P is the applied pressure, and E' is the effective Young modulus for two elastic bodies in contact, and Shigleys cone pressure distribution [12] of bolted joints, which yields the pressure values used in Eq. 4:

$$P(r) = \frac{F}{\pi(r_0^2 - r^2)} \qquad r_i \leq r \leq r_o \quad , \tag{5}$$

where F is the axial force applied by the screw, and r_i and r_0 are the radii of influence of the bolt. Further discussion of Eqs. 4 and 5, and their use is given in Appendix D.

IV. RADIATIVE ENVIRONMENT

The external thermal environment and orbital parameters of ^{Po}Cat-3 depend on both mission requirements and launcher specifications. To cover the full range of possibilities, the most critical cases are simulated, encompassing moderate conditions within them. Table III and the list below summarize the variables, as sourced from the mission requirements [3], [13] and [14], that define each scenario.

- **Perigee height:** From 450 km to 500 km.
- **Eccentricity (e):** Zero
- **Inclination (i):** From 80° to 100°.
- **Launch date:** Estimated Q3-2027.

TABLE III: Heating environment parameters

Environment	**G (W/m^2)**	α	**I$_{\mathbf{IR}}$ (W/m^2)**	β (°)
Hot Case	1428	0.40	260	71.8
Cold Case	1316	0.20	240	0
Extreme Hot Case	1428	0.80	261	71.8
Extreme Cold Case	1316	0.05	189	0

Note that the angle denoted as β corresponds to the one between the orbital plane, and the Sun vector, or vector that goes from the center of the Earht to the center of the Sun. The results presented will be those of the regular Hot and Cold Cases.

V. RESULTS

A. Radiative Analysis

Radiative simulations are performed, through Monte-carlo ray-tracing techniques, providing values of the incident flux from the Sun and Earth through reflection and IR emission. A representation of the orbit is shown in Figure 5.

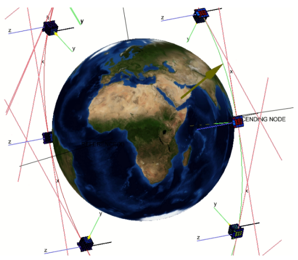

FIG. 5: Visual orbital results representation of sum of flux in different positions.

The simulations presented correspond to the cold and hot cases, as specified in Table III, with a perigee height of 450km, a polar (90°) inclination, and constant β. The spacecraft will be pointing perfectly towards Nadir (P/L antenna facing towards Earth, corresponding to the +Y axis). The system is set to be spinning fast enough so that the four lateral faces receive an equal amount of flux in each position.

Note that for these β angles the PQ will either be in eclipse for 35.77 minutes each orbit or always sunlit.

The sum of fluxes yields the following results for three geometries located in perpendicular planes to each other, the K-band antenna, the bottom solar panel and a lateral solar panel, shown in Figures 6 and 7.

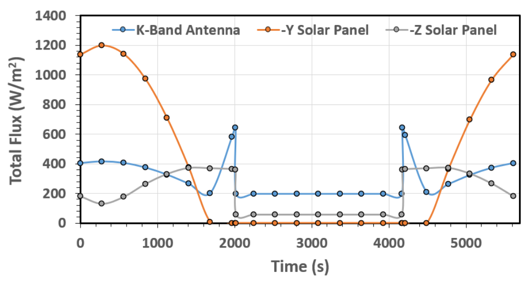

FIG. 6: Sum of fluxes of three orthogonal external geometries for the cold case radiative analysis.

While the radiative transfer results are necessary to perform the thermal analysis, they are not key to the DTR verifications. Despite this, the physical coherence of the obtained values is verified before proceeding into simulations.

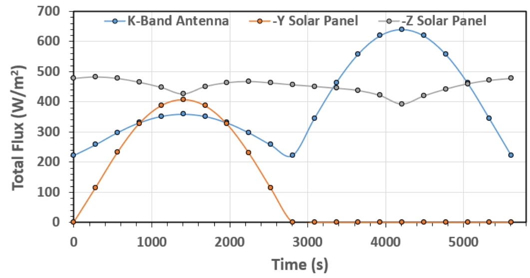

FIG. 7: Sum of fluxes of three orthogonal external geometries for the hot case radiative analysis.

B. Thermal Analysis

Transient cyclic analysis, with a period of two orbits, corresponding to a Survival operational mode of the S/C, under cold case conditions, and a Nominal operational mode, in the hot case have been performed. Being either in Nominal or Survival entails different power consumptions. Therefore, heat loads are calculated and applied to the corresponding geometries.

The cold case considered constitutes the Worst Cold Case (WCC) while the hot case constitutes the Worst Hot Case (WHC). Simulations begin with these cases, being the most constraining possible scenarios, and if in both cases the S/C yields values within the DTRs, the confidence on ^{Po}Cat-3 increases significantly.

Relevant data of the maximum and minimum temperatures of critical geometries is shown in Figures 8 and 9, for the WCC and WHC respectively.

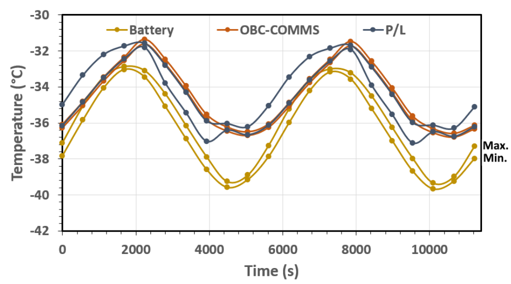

FIG. 8: Minima and maxima temperatures of the battery, OBC-COMMS and K-band PCBs in the WCC.

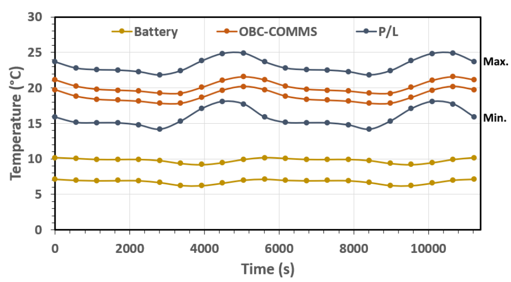

FIG. 9: Minima and maxima temperatures of the battery, OBC-COMMS and K-band PCBs in the WHC.

The predicted minima and maxima temperatures reached, in each of the simulated scenarios, by the subsystems and components showcased in Table I, is presented in Table IV.

TABLE IV: Subsystem Temperature Ranges in the WCC and WHC

Subsystem	Temp. WCC (°C)		Temp. WHC (°C)	
	Min	Max	Min	Max
EPS	-36.85	-31.58	17.81	21.60
AOCS	-37.13	-31.65	17.52	28.39
OBC-COMMS	-36.80	-31.36	20.19	21.60
K-band	-37.12	-31.59	14.17	24.90
Antenna	-37.67	-30.84	11.36	18.55
Lateral Boards	-39.49	-33.41	5.94	7.40
Bottom Board	-40.61	-32.00	3.35	4.61
Battery	-39.68	-32.87	6.21	10.15

By comparing the predicted temperatures with the DTRs, it is determined that adjusting the PQ's external optical properties, through the use of gold or black coatings, is needed to satisfy the battery's thermal requirements under the WHC. In the WCC, despite greatly improving the behavior of the S/C, passive element modifications don't suffice, and installing a heater would not ensure compliance with the DTRs, given the functionality constraints of the Survival operational mode. Consequently, both the software architecture and the power budget must be reassessed to accommodate an active thermal solution.

Results of additional simulations, with more absorbent surfaces than currently used, are presented in Appendix E, and are taken as a basis for the proposed solutions.

VI. CONCLUSIONS

The radiative and thermal behavior of the ^{Po}Cat-3 PocketQube has been analyzed, after the detailed modeling of its physical properties, obtaining flux and temperature distributions for different orbits and heating scenarios.

It has been determined that under the Worst Cold Case the spacecraft would be unable to meet its DRTs without the implementation of an active thermal solution, and that in the Worst Hot Case the battery would require of auxiliary heating to perform its charging, unless the external PCBs coating is replaced with a more infra-red absorbing one. Further transient analyses are required in order to assess wether the spacecraft will meet its requirements over more moderate and probable scenarios, while also testing more optical configurations and active thermal management systems.

Future work would also benefit from including time dependent power consumptions of the integrated circuits, as the minimum and maximum temperatures reached are sure to be impacted by such variation.

Finally, the modeling and approximations taken are novel in PQ development, and as such a TVAC test campaign would be necessary to validate the model and perform correlations to improve further simulations. Despite this they yield reasonable values, showing a path for realistic and accessible thermal analysis.

Acknowledgments

I want to firstly acknowledge the support of the Ksenia Osipova and Luis Contreras Benito, PhD candidates in Aerospace Science and Technology, as well as my advisors Adriano Camps and Anna Maria Vila for their support and guidance. Finnally, I also want to thank Malgorzata Solyga, Thermal Engineer at ESA, for her expertise, advice and feedback, and my colleagues of the ^{Po}Cat-Lektron team, who make this mission possible.

[1] Cal Poly, *CubeSat Design Specification* Rev 14.1, February 2022
[2] Alba Orbital, TU Delft, AUSS, *The PocketQube Standard*, Issue 1, June 2018
[3] UPC NanoSat Lab, *IEEE Open PocketQube Kit Wiki*, September 2024
[4] European Space Agency, *About Fly Your Satellite*, 2024
[5] A. Golkar and I. Lluch i Cruz, *The Federated Satellite Systems paradigm: Concept and business case evaluation*, February 2015
[6] UPC Nanosat Lab, *IEEE UPC-Unite! Basic Course on Small Sats and the IEEE GRSS Open PocketQube Kit*, January 2025
[7] ITP Aero, *ESATAN-TMS Thermal Modeling Suite Website* (https://www.esatan-tms.com/index.php)
[8] European Comission for Space Standarization, *ECSS-E-ST-31C Space Engineering*, Issue 2, 2008/11/15
[9] UPC NanoSat Lab, *IEEE PocketQubes Hardware Repository* (https://github.com/nanosatlab/pocat-hw)
[10] Philipp B. Hagger et al, *Contact Conductance in Common CubeSat Stacks*, September 2024
[11] B. B. Mikic, *Thermal Contact Conductance; Theoretical Considerations*, 1974
[12] Richard G. Budynas and J. Keith Nisbett, *Shigley's Mechanical Engineering Design, Tenth Edition*, 2015
[13] P. D.G. Gilmore, *Spacecraft Thermal Control Handbook: Fundamental Technologies*, 2002
[14] J. Nataly et al, *The 3Cat-4 Spacecraft Thermal Analysis and Thermal Vacuum Test Campaign Results*, September 2024
[15] Albin K J. Hasselström and U. Eskil Nilsson, *Thermal Contact Conductance in Bolted Joints*, 2012

Anàlisi tèrmic del satèl·lit PocketQube ^{Po}Cat-3

Author: Óscar Pavón Amador, opavonam11@alumnes.ub.edu
Facultat de Física, Universitat de Barcelona, Diagonal 645, 08028 Barcelona, Spain.

Advisors: Adriano Camps, Anna Maria Vilà Arbonès

Resum: Aquest Treball de Fi de Grau presenta l'anàlisi tèrmic del ^{Po}Cat-3, un satèl·lit PocketQube 1P. S'avalua el comportament tèrmic de l'instrument, validant els requisits establerts pels seus components electrònics, alhora que es proporciona una base sòlida per a futures anàlisis d'altres IEEE GRSS Open PocketQubes. S'ha desenvolupat un model tèrmic basat en la geometria del satèl·lit, les propietats dels materials i els paràmetres orbitals. Es presenten simulacions en estat transitori per a diferents condicions de contorn. Els resultats obtinguts posen de manifest la necessitat d'un sistema tèrmic actiu i la possible transició d'un recobriment blanc a un de més absorbent, ja que en els escenaris tant freds com càlids no s'ha complert tots els requisits a causa de temperatures predites inferiors a les acceptables.
Paraules clau: Transferència de calor, simulació tèrmica, PocketQube, electrònica, TCR
ODSs: ODS 4, ODS 9, ODS 13

Objectius de Desenvolupament Sostenible (ODSs o SDGs)

1. Fi de les desigualtats		10. Reducció de les desigualtats	
2. Fam zero		11. Ciutats i comunitats sostenibles	
3. Salut i benestar		12. Consum i producció responsables	
4. Educació de qualitat	X	13. Acció climàtica	X
5. Igualtat de gènere		14. Vida submarina	
6. Aigua neta i sanejament		15. Vida terrestre	
7. Energia neta i sostenible		16. Pau, justícia i institucions sòlides	
8. Treball digne i creixement econòmic		17. Aliança pels objectius	
9. Indústria, innovació, infraestructures	X		

Aquest projecte contribueix a una educació de qualitat, oferint suport a futurs estudiants que realitzin anàlisis tèrmics dels seus propis PocketQubes (ODS 4). D'altra banda, se situa a l'avantguarda del desenvolupament de la tecnologia de picosatèl·lits, ampliant el ventall de possibilitats d'aquestes innovadores plataformes (ODS 9). Finalment, les mesures obtingudes amb el satèl·lit permetran caracteritzar interferències amb les mesures de vapor atmosfèric, un forçador climàtic de gran importància (ODS 13).

GRAPHICAL ABSTRACT

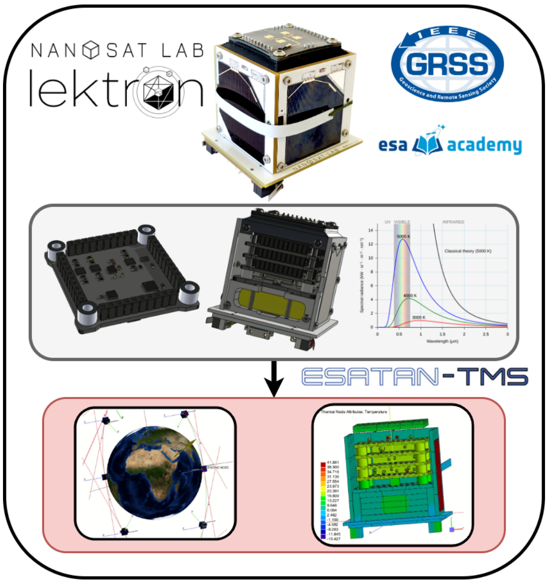

Appendix A: Operational Modes

The satellites' state machine can be in one of four operational modes: Init, Nominal, Contingency and Survival. The tasks that ^{Po}Cat-3 can perform will decrease with battery levels, in order to avoid complete depletion. Figure 10 presents the state machine:

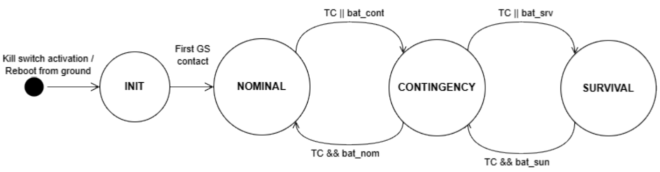

FIG. 10: Operational Modes Diagram

Power consumption is highest in a Nominal operational mode, and it decreases significantly in Contingency and further in Survival. The amount of heat generated inside the PQ is proportional to power consumption and therefore is considered when analyzing the thermal behavior of the S/C. In Table V an estimation of each operational modes power consumption and functionalities is provided:

TABLE V: Operational modes permitted actions and estimated power consumption

Action	**Init**	**Nominal**	**Contingency**	**Survival**
COMMS TX	Yes	Yes	Yes	No
COMMS RX	Yes	Yes	Yes	No
AOCS Detumbling	Yes	Yes	No	No
AOCS Nadir Pointing	No	Yes	No	No
Payload Experiment	No	Yes	No	No
FSS Services	No	Yes	No	No
EPS Heating	No	Yes	Yes	No
Power (mWh)	74	995	72	46

Appendix B: Material Properties Calculations

- **IR emissivity** ($\varepsilon_{\mathbf{IR}}$): The IR emissivity is computed by performing a weighted average, by projected surface, of the conjunction of pieces modeled.

$$\varepsilon_{IR} = \sum_i \frac{A_i \cdot \varepsilon_i}{A_T} \quad , \tag{B1}$$

where A_T denotes the sum of all projected areas.

- **Solar Absorptivity** ($\alpha_{\mathbf{s}}$): Solar Absorptivity is calculated following the same procedure as for the IR emissivity:

$$\alpha_s = \sum_i \frac{A_i \cdot \alpha_i}{A_T} \tag{B2}$$

- **Density**(ρ): The density is computed by dividing the mass of the real component or components by the volume of the ESATAN primitive defined.

$$\rho = \frac{m_{real}}{V_{primitive}} \tag{B3}$$

- **Specific Heat** ($\mathbf{c_p}$): The specific heat is computed as the weighted sum of the individual specific heats by mass of each real component:

$$c_p = \sum_i \frac{c_i \cdot m_i}{m_T} \quad , \tag{B4}$$

where m_T denotes the sum of all masses. Due to the impossibility of measuring each layers' mass we can make use of its relation with density and volume such that:

$$m_i = V_i \cdot \rho = l_i \cdot A_i \cdot \rho_i \quad , \tag{B5}$$

where l_i and A_i denote the length and area of the layer, respectively. Coming back to expression (7) we finally obtain:

$$c_p = \sum_i \frac{l_i \cdot A_i \cdot \rho_i \cdot c_p^i}{\sum_j l_j \cdot A_j \cdot \rho_j} \tag{B6}$$

As the area is equal for each layer we can extract it from the summation, resulting in:

$$c_p = \sum_i \frac{l_i \cdot \rho_i \cdot c_p^i}{\sum_j l_j \cdot \rho_j} \tag{B7}$$

- **Conductivity**($\mathbf{k}$): The in-plane conductivity:

$$\kappa_{i.p.} = \sum_i \frac{\kappa_i \cdot l_i}{l_T} \tag{B8}$$

Where κ_i denotes the in-plane conductivity of each material, l_i its thickness, and l_T the total thickness of the PCB. The cross-plane conductivity:

$$\kappa_{c.p.} = \left(\sum_i \frac{l_i}{\kappa_i} \right)^{-1} \cdot l_T \tag{B9}$$

Appendix C: Thermal Model

1. Geometrical Model

The thermal geometrical model is curated by simplifying a highly detailed CAD model designed in SolidWorks [9]. The parts of the spacecraft are defined in ESATAN-TMS manually, approximating shapes and volumes to either rectangular boxes or cylinders. Small elements as dents, holes, lateral board screws and cables have not modeled in ESATAN, assuming their weak influence on the behavior of $^{\text{Po}}$Cat-3, yet are taken into account when computing macroscopic properties, such as specific heat and conductivity.

Different views of the elaborated model are provided in the following figures, with the intent of giving a grasp on the performed approximations. The battery inside its support is shown in Figure 11:

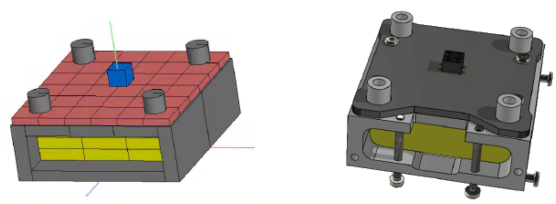

FIG. 11: Comparison of the battery within its support, with the +Y magnetorquer on top.

The bottom board, -Y solar panel and killswitches are shown in Figure 12, all modeled as solid rectangular prisms:

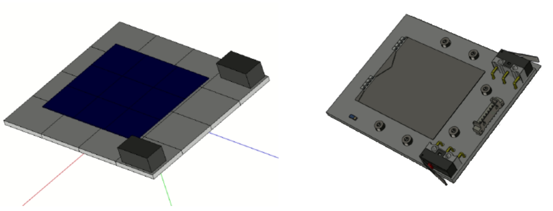

FIG. 12: Comparison of the bottom board, with solar panel and killswitches.

The vertical connectors, which electrically connect the PCBs in the stack, are shown in Figure 13, also simplified to rectangular prisms:

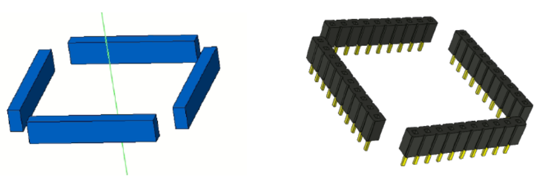

FIG. 13: Comparison of the vertical connectors.

The threaded spacers are modeled as solid cylinders, while the screws are modeled into the properties of the spacers primitives, with an added G_L between them to represent the heat path through the screws. Their comparison is shown in Figure 14:

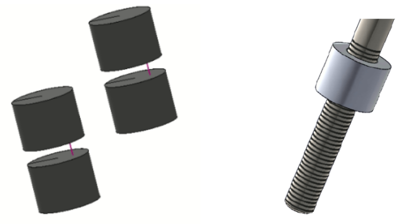

FIG. 14: Comparison of spacers. Two sets of spacers are shown on the left (ESATAN) while a threaded spacer is shown on the right.

The K-band payload, along with its support, has been modeled by a combination of rectangular prisms. The heat path provided by the non-modeled screws and vertical connectors has been included by the addition of UDCs, calculated as defined in Eq.3. In Figures 15 and 16 the geometries are presented:

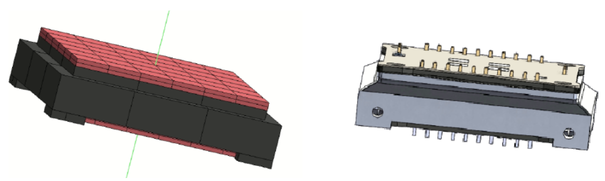

FIG. 15: Comparison of the K-band payload, including antenna and mechanical support.

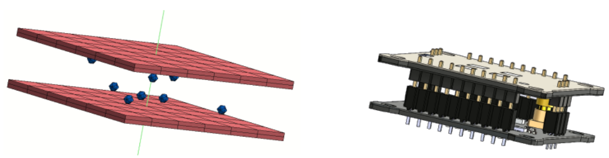

FIG. 16: Comparison of the K-band payload without mechanical support.

2. Bulk and optical properties

Each one of the defined primitives has a corresponding set of macroscopic (bulk) and optical properties. The values, presented in Table VI of infrared emissivity (ε_{IR}), solar absorptivity (α_s), density (ρ), specific heat (c_p), and conductivity (κ) have been used as basis for properties' calculation:

It has been considered, unless otherwise stated, that all internal PCBs have black paint properties, while outside PCBs (lateral, slider and bottom boards) have white paint optical properties, with the values presented in Table VI.

TABLE VI: Bulk and optical properties of used materials

Material	ε_{IR}	α_s	ρ (kg/m^3)	c_p (J/kg·K)	k (W/m·K)
FR-4 (in-plane)	0.94	0.12	1850	1200	0.81)
FR-4 (cross-plane)	0.94	0.12	1850	1200	0.29
Copper	x	x	8930	385	400.00
Teflon (PFTE)	0.92	0.05	2070	1010	0.27
Stainless Steel (AlSl304SS)	0.08	0.42	8000	500	15.00
Aluminum Alloy (7075)	0.21	0.18	2810	960	130.00
RSRogers	x	x	2200	960	0.20
LiPo Battery	0.30	0.50	2750	1000	1.50
Phosphor Bronze	x	x	8800	380	62.00
Aluminum 6063-T5	0.77	0.80	2700	900	209.00
Gallium Arsenide	0.85	0.91	5316	325	50.00
ABS (Plastic)	0.82	0.94	1070	1990	0.16
White Paint	0.94	0.19	x	x	x
Black Paint	0.94	0.96	x	x	x

Appendix D: Thermal Contact Resistance Calculations

The first step taken to calculate the TCR is to determine the pressure at the interface between the two surfaces. Shigleys conical pressure distribution [12] establishes:

$$P(r) = \frac{F}{\pi(r_0^2 - r^2)} \qquad r_i \leq r \leq r_o \tag{D1}$$

Here r_i is simply the inner diameter of the bolt while r_0 denotes the outer radii of influence of the applied force, considering that is spreads as a cone with an angle of 30°:

$$r_o = xtan(\alpha) + \frac{D}{2} \tag{D2}$$

Here x denotes the depth from the upper outer surface of the fist body, where the screw's head lies and, $\alpha = 30$ and D is the outer diameter of the used screw. Now, in order to calculate the force applied by the screw we use:

$$F = \frac{\tau_{tot}}{0.16P_T + 0.58\mu d_2 + \mu_b r_m} \quad . \tag{D3}$$

In this expression τ_{tot} corresponds to the applied torque, P_T to the thread pitch, $r_m = \frac{d+D}{4}$, being d and D the diameters of the hole and bolt head respectively, and μ and μ_b are assumed to be equal friction coefficients with an approximate value of $\mu = \mu_b \approx 0.225$.

Chosen due to its practicality with respect to other models, Mikic's equation establishes that:

$$h_c = 1.55\frac{k_s m_s}{\sigma_s}\left(\frac{P\sqrt{2}}{E' m_s}\right) \quad , \tag{D4}$$

and the rest of the parameters:

$$k_s = \frac{2k_1 k_2}{k_1 + k_2} \quad , \tag{D5}$$

where k_1 and k_2 are the materials cross plane conductivities.

$$\sigma_s = \sqrt{\sigma_1^2 + \sigma_2^2} \quad , \tag{D6}$$

$$\sigma_i = \sqrt{\frac{\pi}{2}}R_a \quad , \tag{D7}$$

where R_a is the average roughness of the piece as established by the manufacturer, and σ_s denotes the RMS surface roughness assuming a Gaussian distribution of asperities.

Then, m_s can be simplified to $m_s = 0.1$ because of its small influence on h_c, and becouse it is a good approximation for blasted surfaces [15].

Now, in order to calculate E' we use:

$$E' = \frac{E_1 E_2}{E_2(1-\nu_1^2) + E_1(1-\nu_2^2)} \quad , \tag{D8}$$

where E_i is the Young modulus, and ν_i the Poisson ratio. However, due to the fact that the PCBs are made of different materials we have to estimate the modulus and ratios for the composite as:

$$\frac{1}{E_i} = \frac{1}{l_T}\sum_m \frac{l_m}{E_m} \quad , \tag{D9}$$

$$\frac{1}{\nu_i} = \frac{1}{l_T}\sum_m \frac{l_m}{\nu_m} \quad , \tag{D10}$$

where E_m and ν_m denote the Young's modulus and ratio of each material, l_m denotes the length of the layer of said material and l_T the total length of the solid.

Finally, taking into account the fact that only a small portion of the surfaces is under pressure, and that ESATAN considers the whole interface area, we weight the value by the total area.

$$\bar{h_c} = \frac{A_{pressure}}{A_{interface}} \cdot h_c \quad , \tag{D11}$$

yielding the values used in the thermal model, which range from 100 $W/m^2 \cdot K$ to 2000 $W/m^2 \cdot K$.

Despite being theoretically able to use this approach for all bolted interfaces, it is evident that a screw that connects multiple interfaces is not easy to model. Therefore, the values of the inner stack TCR for spacers are extrapolated from [10] by choosing the closest configuration to us and accounting for torque differences as established in the paper. The calculated TCR value is then of 6980 $W/m^2 \cdot K$.

Appendix E: Additional Radiative and Thermal Simulations

The presented simulations Section V correspond to a PQ modeled as close to current design as possible. As the results obtained showcase lower than required temperatures, additional simulations have been performed, changing the external coating of the satellite to a more absorbent one, assuming the optical properties of black paint from Table VI for the lateral, bottom and slider boards.

The results of the thermal analysis are presented in Figures 17 and 18:

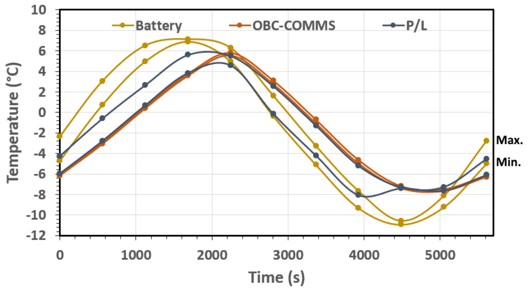

FIG. 17: Minima and maxima temperatures of the battery, OBC-COMMS and K-band PCBs in the WCC, with external black coating.

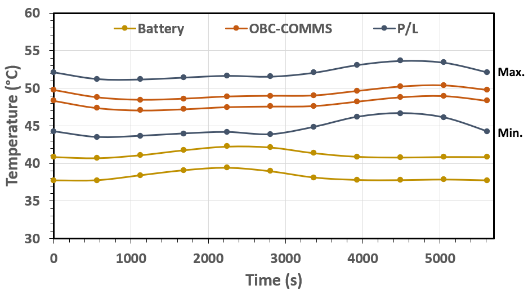

FIG. 18: Minima and maxima temperatures of the battery, OBC-COMMS and K-band PCBs in the WHC, with external black coating.

Visualizing the temperature distribution, in the WCC, of the nodes at a time of 1684 seconds of the white and black coated models in Figures 19 and 20:

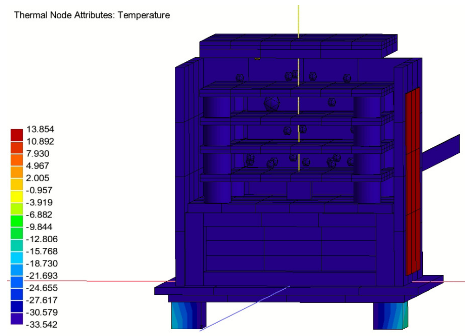

FIG. 19: Temperature distribution of the model nodes in a WCC, white coatings.

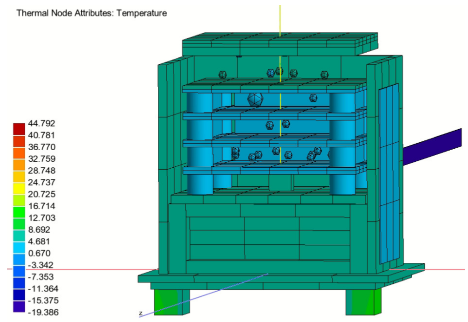

FIG. 20: Temperature distribution of the model nodes in a WCC, black coatings.

A great improvement can be observed in the temperatures of the S/C, reinforcing the idea of using black coatings.